Title

Photoredox Catalysis with Spin Magnetic Field Effects: A Scheme for Chiral Resolution

Journal

Journal of the American Chemical Society, 147(40)

ISSN

0002-7863

Authors

Poh, Yong Rui

Koner, Arghadip

Reitz, Michael

et al.

Publication Date

2025-10-08

DOI

10.1021/jacs.5c11502

JACS
JOURNAL OF THE AMERICAN CHEMICAL SOCIETY
pubs.acs.org/JACS
Article

Photoredox Catalysis with Spin Magnetic Field Effects: A Scheme for Chiral Resolution

Yong Rui Poh,*[,‡] Arghadip Koner,[‡] Michael Reitz, and Joel Yuen-Zhou*

Cite This: J. Am. Chem. Soc. 2025, 147, 36579−36588
Read Online

ABSTRACT: Quantities that break both mirror symmetry and time-reversal symmetry, such as the orbital angular momentum, are known to connect molecular chirality with an applied magnetic field. This concept has led to observations such as magneto-chiral dichroism and chirality-induced spin selectivity (CISS). However, being small, these effects often require additional amplification procedures such as flow chemistry to achieve bulk enantioseparation. In this work, we demonstrate how the magnetic field effect on photogenerated radical pairs, which also breaks time-reversal symmetry, can be harnessed for enantiopurification. Fundamental to this process is the collective decay of the singlet and triplet radical-pair states made possible by an applied magnetic field. Because opposite enantiomers exhibit spin−orbit coupling matrix elements of opposite signs, the singlet and triplet decay channels interfere constructively in one enantiomer. Meanwhile, molecules of the other enantiomer are funnelled into the first enantiomer through excited-state chirality inversion, achieving (dynamic kinetic) chiral resolution. Using an axially chiral binaphthyl derivative and a borane photosensitizer as prototype, we predict an appreciable enantiomeric excess (e.e.) of 90% to be possible at steady state, attained within hundreds of milliseconds when irradiated by a laser. Importantly, our analytical results showcase regimes of perfect enantioselectivity (100% e.e.), accessible by further chemical optimization of the photosensitizer for which general strategies are discussed. Overall, this work illustrates a so-far untapped but powerful control knob for photoredox catalysis based on spin chemistry principles.

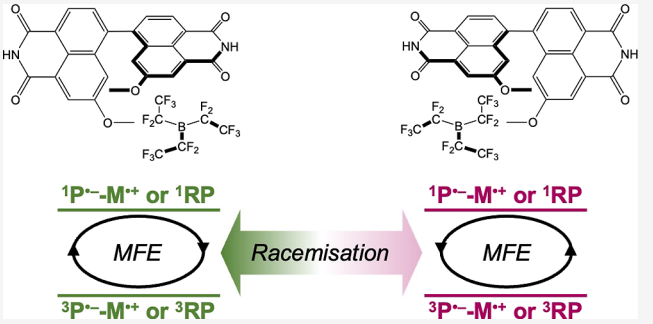

INTRODUCTION

Most photochemical reactions generate pairs of radical intermediates,[1−7] a phenomenon known as chemically induced dynamic electron polarization (CIDEP).[8] These spin-correlated radical pairs (RPs) can then evolve coherently among the singlet and triplet basis states, often influenced by an applied magnetic field through the spin Zeeman effect. Because the singlet states react differently from the triplet states, their average populations can be detected by the ensuing chemical kinetics, leading to techniques such as reaction yield-detected magnetic resonance.[8] Such magnetic field effects (MFEs) have been proposed as explanations for magnetoreception[9−12] with potential applications ranging from light harvesting to quantum sensing.[13−15]

Adjacent to this field is the study of chirality-induced spin selectivity (CISS), a more-recently discovered effect that also polarizes electron spins.[16] This is achieved by passing an electron current through a chiral molecule or material, thereby relating the electron's magnetization with the (geometric) chirality.[17−21] The CISS effect has been observed in various forms including photoemission,[22−24] electron transport,[25−28] and transient charge polarization.[29−31] Its theoretical foundations are still being investigated,[17] most of which point toward the role of chiral vibrations or phonons that couple to the electron spins through non-Born−Oppenheimer effects.[32−45]

Beyond observations of CISS, the same effect has also been harnessed to discriminate enantiomers using polarized electron spins,[46−48] uncovering new prospects for chiral resolution[49−54] and possibly new understanding of life's homochirality.[53,55,56] While remarkable, this direction has so far been limited to the enantioselective adsorption of amino acids and small peptides onto magnetized surfaces.[49,52,54] To attain bulk separation, amplification processes such as flow reactions and crystallization are required,[49−51,53] implying some restrictions in its synthetic applicability, although there is much potential for theoretical developments to guide the rational design of CISS-based separation systems.[54,57−59] From there, benchmarks can be made against other spin-based techniques; for instance,

Received: July 8, 2025
Revised: September 11, 2025
Accepted: September 11, 2025
Published: September 26, 2025

https://doi.org/10.1021/jacs.5c11502
J. Am. Chem. Soc. 2025, 147, 36579−36588

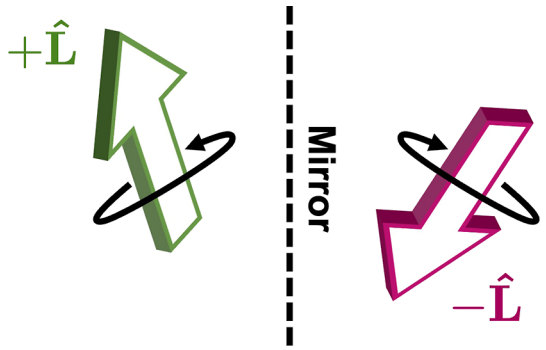

Figure 1. OAM $\hat{\mathbf{L}}$, being an axial vector, changes direction in the mirror image, connecting it with its time-reversed counterpart.

photon spins are also known to discriminate enantiomers, albeit with a small enantiomeric excess (e.e.) of <1%.[60−64]

In this work, we offer a novel spin-based enantioseparation technology by utilizing the MFE of radical pairs to invoke chiral resolution. The connection is achieved via the electron orbital angular momentum (OAM; labeled $\hat{\mathbf{L}}$). Being odd under both time-reversal symmetry (TRS) and mirror reflection,[65] the OAM is time-reversed in opposite enantiomers [Figure 1]. Hence, a process that breaks TRS, such as the introduction of a magnetic field **B**, will also separate the two enantiomers. For instance, the *orbital* Zeeman coupling ($\sim\mathbf{B}\cdot\hat{\mathbf{L}}$) flips sign under mirror reflection, causing one enantiomer to absorb *linearly* polarized light more strongly than the other; this phenomenon is termed magneto-chiral dichroism.[26,66−74] Unfortunately, the effect is weak resulting in an experimental e.e. of <0.1%,[69] mainly because the *orbital* Zeeman term in molecules is small relative to the typical orbital (i.e., electronic) energy separation.[71,73,74] By converting the OAM into spin angular momentum (SAM; labeled $\hat{\mathbf{S}}$) through a spin−orbit coupling (SOC), we propose the use of the *spin* Zeeman effect, the energy of which can be larger than the spin-intrinsic zero-field splitting (ZFS). This way, the time-reversed pair of SAM acts as a proxy for the two enantiomers through the OAM.

While the total orbital-spin angular momentum is known to link mirror symmetry to TRS,[65,75,76] its application toward enantioselective photoredox catalysis through the *spin* Zeeman effect is, to our best knowledge, unprecedented. In our proposal, we shall distinguish the time-reversed SAMs by coherently evolving one of the photoinjected triplet M_S sublevels with the singlet state using a magnetic field, an implementation of the MFE [Figure 2]. The subsequent collective singlet−triplet decay of the RP to the ground state will be faster in one enantiomer due to constructive interference between the electronic and spin−orbit channels. Therefore, at steady state, chiral resolution can be achieved in molecules that racemise faster in an oxidized or reduced state. Importantly, our analytical solutions show regimes of perfect enantioselectivity (i.e., an e.e. of 100%) to be accessible by chemical fine-tuning. For instance, the RP formed between an axially chiral binaphthyl derivative and a borane photosensitizer [Figure 2] displayed an e.e. of 90% at steady state, a signficant improvement from the <1% e.e. obtained via other magnetochiral methods.[46−48,69] Further, enantiopurification is achieved with a time scale of hundreds of milliseconds under a laser light source, which is experimentally feasible. Techniques for further improvement will also be discussed.

RESULTS AND DISCUSSIONS

The Chiral Resolution Protocol. Our photoredox catalysis setup for enantiopurification comprises a photosensitizer (i.e., a photocatalyst) and a racemic mixture of chiral molecules [Figure 2]. The photosensitizer is first excited from its singlet ground state, $|^1\mathrm{GS}\rangle$ (GS = ground state), to a *triplet* excited state, $|^3\mathrm{LE}\rangle$ (LE = local excitation), made possible by strong SOCs in the photosensitizer (more to follow). The

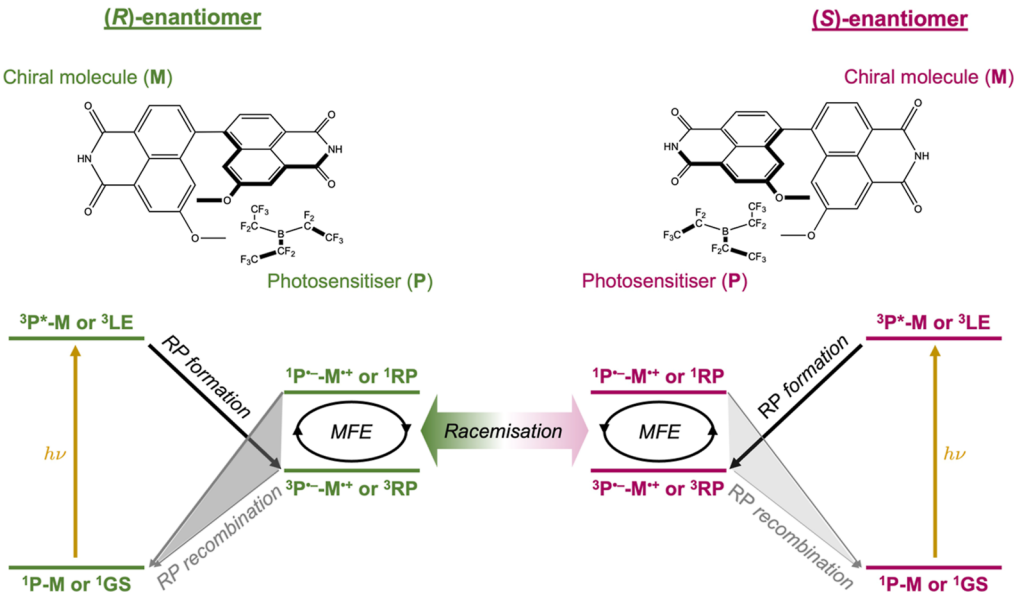

Figure 2. An overview of the spin-based enantioseparation scheme. In general, chiral molecules are destabilized and racemise faster in their oxidized/reduced ionic states. In this scheme, we first form a triplet RP between a photosensitizer and the chiral molecule by optical spin injection. This triplet RP then picks up a small amount of singlet character due to the MFE. The ensuing singlet−triplet coherence sets up a constructive interference between the singlet and triplet decay channels in one enantiomer, causing its RP to recombine more quickly. The other enantiomer, having spent more time in the (ionic) RP state, has a higher chance of inverting its chirality, leading to chiral resolution at steady state.

https://doi.org/10.1021/jacs.5c11502
J. Am. Chem. Soc. 2025, 147, 36579−36588

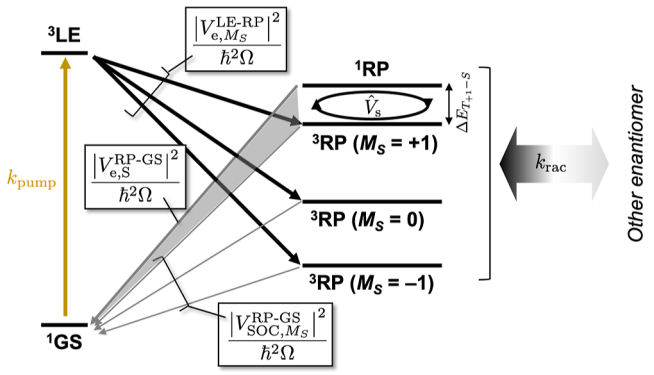

Figure 3. Summary of the excited-state kinetics and their associated rates or operators.

photoexcited state then undergoes a subnanosecond electron transfer to the chiral molecule to form a RP in the *triplet* state, $|^3\mathrm{RP}\rangle$. Subsequently, this triplet RP state mixes with the singlet RP state, $|^1\mathrm{RP}\rangle$, through a weak external magnetic field. All four RP states (one singlet and three triplets) can decay independently to the $|^1\mathrm{GS}\rangle$ state, and we shall denote their rates by

$$w_T = \frac{1}{\hbar^2\Omega}|V_{SOC,M_S}^{RP\text{-}GS}|^2 \tag{1}$$

for the triplet M_S sublevel $|^3\mathrm{RP};M_S\rangle$, and

$$w_S = \frac{1}{\hbar^2\Omega}|V_{e,S}^{RP\text{-}GS}|^2 \tag{2}$$

for the singlet state $|^1\mathrm{RP}\rangle$ [Figure 3]. Here, $V_{e,S}^{RP\text{-}GS}$ and $V_{SOC,M_S}^{RP\text{-}GS}$ are, respectively, the real-valued electronic and complex-valued spin−orbit couplings responsible for the singlet and triplet RP recombination, while the prefactor $(\hbar^2\Omega)^{-1}$ is a proportionality constant that encapsulates the bath interactions (see footnote[1]). eqs 1 and 2 require the RP states to be the lowest-lying excitations of the system (otherwise the triplet RP can decay into other lower-energy triplet states[14]). To satisfy that, we can use photosensitizers with HOMOs (or LUMOs) that are close in energy to the chiral molecule's LUMO (or HOMO), thereby minimizing the energy for electron transfer (HOMO = highest occupied molecular orbital; LUMO = lowest unoccupied molecular orbital).

If one of the triplet M_S RP sublevels is now brought into near-degeneracy with the singlet RP state, then their quantum coherence allows the two states to decay collectively. For instance, if the singlet RP state were to be higher in energy than its triplet counterpart, then a magnetic field can bring the $|^3\mathrm{RP};+1\rangle$ state into near-degeneracy with the $|^1\mathrm{RP}\rangle$ state, yielding the following perturbed state (Supporting Information S1)

$$\overline{|^3\mathrm{RP};+1\rangle} \approx |^3\mathrm{RP};+1\rangle + |^1\mathrm{RP}\rangle\left[\frac{\langle^1\mathrm{RP}|\hat{V}_s|^3\mathrm{RP};+1\rangle}{\Delta E_{T_{+1}-S}}\right] \tag{3}$$

where $\Delta E_{T_{+1}-S} \equiv E(^3\mathrm{RP};+1) - E(^1\mathrm{RP})$ is the energy difference between the near-degenerate states and $\hat{V}_s$ is the spin Hamiltonian for a RP. The collective decay rate $w_+^{(R)}$ between these two states will be approximately

$$w_+^{(R)} \approx \frac{1}{\hbar^2\Omega}\left|V_{SOC,+1}^{RP\text{-}GS} + V_{e,S}^{RP\text{-}GS}\left[\frac{\langle^1\mathrm{RP}|\hat{V}_s|^3\mathrm{RP};+1\rangle}{\Delta E_{T_{+1}-S}}\right]\right|^2 \tag{4}$$

To understand the origin of the chiral resolution, let us denote eq 4 as the rate for the (R)-enantiomer. Its mirror image—the (S)-enantiomer—will experience a similar rate but with an opposite sign on $V_{SOC,+1}^{RP\text{-}GS}$

$$w_+^{(S)} \approx \frac{1}{\hbar^2\Omega}\left|-V_{SOC,+1}^{RP\text{-}GS} + V_{e,S}^{RP\text{-}GS}\left[\frac{\langle^1\mathrm{RP}|\hat{V}_s|^3\mathrm{RP};+1\rangle}{\Delta E_{T_{+1}-S}}\right]\right|^2 \tag{5}$$

This is because $V_{SOC,+1}^{RP\text{-}GS}$ is a matrix element of the SOC operator $\sim\hat{\mathbf{L}}\cdot\hat{\mathbf{S}}$, and $\hat{\mathbf{L}}$, being an axial vector [Figure 1], picks up a negative sign under mirror reflection. (Note that, in this work, $\hat{\mathbf{S}}$ stays aligned with $\hat{\mathbf{B}}$, while $\hat{\mathbf{B}}$ follows the symmetry of the electron transfer vector, which is a polar vector; this is consistent with refs 65, 75 and 76). Notice that where the two terms add up in eq 4, the same elements are subtracted in eq 5, and vice versa. This is a manifestation of the interference effect during collective singlet−triplet decay. The enantiomer experiencing a destructive interference will be funnelled into its mirror-reflected counterpart because the barrier to chirality inversion is lower in the RP, which represents a less-stable oxidized/reduced state of the enantiomers. In other words, dynamic kinetic resolution is achieved, which is more valuable than traditional chiral resolution protocols because all molecules of a racemic mixture may, in principle, be converted into an enantiopure compound. Since the steady-state e.e. depends on the differential decay rates $w_+^{(R)}/w_+^{(S)}$, it does not vary much with the rate of chirality inversion.

Note that the triplet RP state decays more slowly than the singlet RP state (i.e., $|V_{SOC,+1}^{RP\text{-}GS}| \ll |V_{e,S}^{RP\text{-}GS}|$), thus the amplitude of the triplet component in eq 3 must be larger than the singlet component for the interference in eqs 4 and 5 to be appreciable. Put differently, there must be a small, yet appreciable, energy separation between the $|^3\mathrm{RP};+1\rangle$ and $|^1\mathrm{RP}\rangle$ states, such that the $|^3\mathrm{RP};+1\rangle$ state contains only a perturbative admixture of $|^1\mathrm{RP}\rangle$ character. This justifies the use of perturbation theory in eq 3, and also explains our choice for a spin-forbidden triplet photoexcitation, which would require a sufficiently strong SOC to occur.[82,83] For our photosensitizer prototype, this transition occurs within 1 day under a mercury lamp and can be down to a microsecond using a regular laser[84]—see Supporting Information S2.

While we have used the $|^3\mathrm{RP};+1\rangle$ state as an example, the $|^3\mathrm{RP};-1\rangle$ state can also be in near-degeneracy with the $|^1\mathrm{RP}\rangle$ state by reversing the magnetic field direction, yielding analogous expressions $w_-^{(R/S)}$ for the collective decay rate. Other than that, no collective decay occurs because the interfering states must be separated by an energy (in frequency units) smaller than the overall decay rate, a consequence of the energy uncertainty due to lifetime broadening[80,81,85] (Supporting Information S1). The chiral resolution χ, defined as the ratio of (R)-enantiomers to (S)-enantiomers at steady state, is characterized by the differential decay rates to be

$$\chi \approx \frac{w_+^{(R)}}{w_+^{(S)}} \times \frac{w_-^{(R)}}{w_-^{(S)}} \tag{6}$$

https://doi.org/10.1021/jacs.5c11502
J. Am. Chem. Soc. 2025, 147, 36579−36588

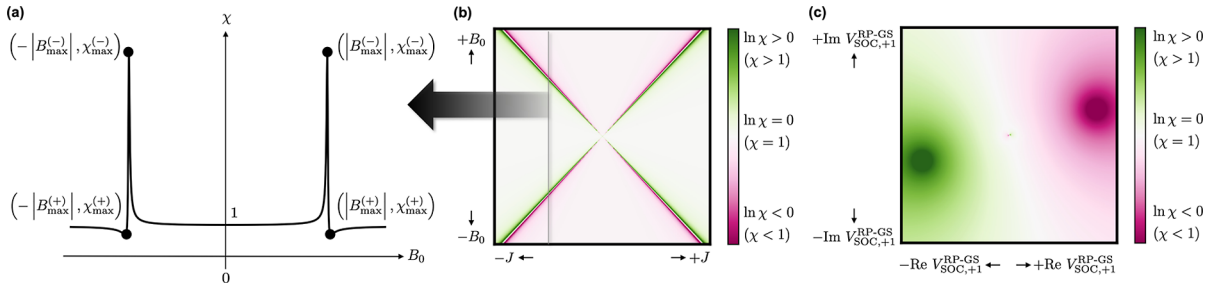

Figure 4. Schematic diagrams of the analytical solution to the chiral resolution χ [eq 6] as a function of (a) the magnetic field strength, B_0, (b) the RP singlet−triplet gap, parametrized by J, and (c) the real and imaginary parts of the SOC matrix element $V_{\mathrm{SOC},+1}^{\mathrm{RP\text{-}GS}}$ responsible for the triplet RP decay. In (c), the quantity $\ln\chi$ diverges (i.e., the e.e. reaches 100%) when $\pm V_{\mathrm{SOC},+1}^{\mathrm{RP\text{-}GS}} = V_{\mathrm{e,S}}^{\mathrm{RP\text{-}GS}}[\langle {}^1\mathrm{RP}|\hat{V}_s|{}^3\mathrm{RP};+1\rangle/\Delta E_{T_{+1}-S}]$. This is represented by the two large dots.

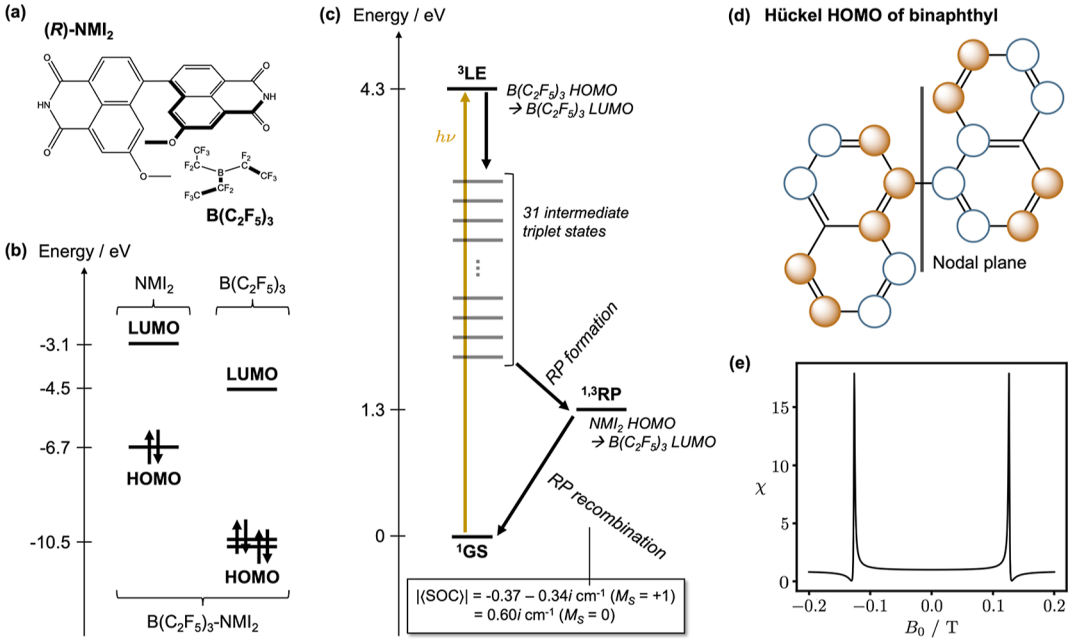

Figure 5. (a) Molecular structures of the model photosensitizer $B(C_2F_5)_3$ and the chiral molecule NMI_2. (b) Energies of the frontier MOs of $B(C_2F_5)_3$ and NMI_2, obtained using two separate DFT calculations (one for each fragment). (c) Excited-state electronic structure, calculated using TDDFT, along with our proposed excited-state relaxation pathway. Also indicated are $V_{\mathrm{SOC},M_S}^{\mathrm{RP\text{-}GS}}$, the SOC matrix elements between the lowest triplet state (i.e., the triplet RP state) and the ground singlet state. (d) Diagrammatic representation of the Hückel HOMO of binaphthyl, which mimicks the chiral molecule NMI_2. (e) Plot of the chiral resolution χ against the magnetic field strength B_0, obtained using the analytical solution presented in eq 6.

where the multiplication arises because the factors $w_+^{(R)}/w_+^{(S)}$ and $w_-^{(R)}/w_-^{(S)}$ deviate most significantly from one in the positive and negative magnetic field regimes, respectively (Supporting Information S1). To further illustrate the enantioseparation, we consider only the spin Zeeman terms $\mu_B\mathbf{B}\cdot\mathbf{g}_j\cdot\hat{\mathbf{S}}_j$ and a singlet−triplet exchange coupling $2J\hat{\mathbf{S}}_A\cdot\hat{\mathbf{S}}_B$ in the spin Hamiltonian (j = A, B labels the radicals in the RP and the remaining terms have their usual meanings). We shall also assume $\mathbf{B} = B_0\mathbf{z}$ ($\mathbf{z}$ is the unit vector along the z-direction) to be aligned with $\mathbf{g}_A$'s principal axis. Denoting $\Delta\mathbf{g} \equiv \mathbf{g}_B - \mathbf{g}_A$ as the difference in g-tensors, we find that (Supporting Information S1)

$$\Delta E_{T_{+1}-S} = 2\hbar^2 J + \hbar\mu_B g_{\mathrm{eff}} B_0 \tag{7}$$

$$\langle {}^1\mathrm{RP}|\hat{V}_s|{}^3\mathrm{RP};+1\rangle = \hbar\mu_B \Delta g_{\mathrm{eff}} B_0 \tag{8}$$

where $g_{\mathrm{eff}} \equiv g_{A,zz} + \Delta g_{zz}/2 \approx 2$ represents an effective electron spin g-factor and $\Delta g_{\mathrm{eff}} \equiv (\Delta g_{zx} + i\Delta g_{zy})/2\sqrt{2}$ denotes an effective difference in the g-tensors (i.e., the MFE). These expressions can be substituted into eqs 4−6 to obtain an analytical expression for the chiral resolution χ (Supporting Information S1). For instance, the enantioenrichment can be controlled by the magnetic field strength B_0, as shown in Figure 4a. For both $B_0 > 0$ and $B_0 < 0$, two extrema are obtained at

$$\chi_{\max}^{(\pm)} = \frac{|\Delta g_{\mathrm{eff}}||V_{\mathrm{SOC},+1}^{\mathrm{RP\text{-}GS}}| \pm \mathrm{Re}\,(\Delta g_{\mathrm{eff}}^* V_{\mathrm{SOC},+1}^{\mathrm{RP\text{-}GS}})}{|\Delta g_{\mathrm{eff}}||V_{\mathrm{SOC},+1}^{\mathrm{RP\text{-}GS}}| \mp \mathrm{Re}\,(\Delta g_{\mathrm{eff}}^* V_{\mathrm{SOC},+1}^{\mathrm{RP\text{-}GS}})} \tag{9}$$

$$B_{\max}^{(\pm)} = \frac{2(\hbar J/\mu_B)|V_{\mathrm{SOC},+1}^{\mathrm{RP\text{-}GS}}|}{\pm|\Delta g_{\mathrm{eff}}|V_{\mathrm{e,S}}^{\mathrm{RP\text{-}GS}}| - g_{\mathrm{eff}}|V_{\mathrm{SOC},+1}^{\mathrm{RP\text{-}GS}}|} \tag{10}$$

https://doi.org/10.1021/jacs.5c11502
J. Am. Chem. Soc. 2025, 147, 36579−36588

each corresponding to a *near*-perfect constructive interference in a specific enantiomer. (Note that in eqs 9 and 10, "±" labels the two extrema rather than the sign of B_0.) Notice how $\chi_{\max}^{(\pm)}$ approaches either zero or infinity (i.e., perfect enantioseparation is achieved with 100% e.e.) when both Δg_{eff} and $V_{\text{SOC},+1}^{\text{RP-GS}}$ are purely real or purely imaginary. Indeed, this implies that the terms in either eqs 4 or 5 *perfectly* cancel out at some magnetic field strength B_0. Importantly, Δg_{eff} and $V_{\text{SOC},+1}^{\text{RP-GS}}$ both depend on some SOC matrix elements.[8] For instance, the elements of the g-tensor may be approximated by second-order perturbation theory in the SOC to be[8]

$$g_{ab} = g_e\delta_{ab} + 2\lambda \sum_{\Psi'} \frac{\langle\Psi|\hat{L}_a|\Psi'\rangle\langle\Psi'|\hat{L}_b|\Psi\rangle}{E_\Psi - E_{\Psi'}} \tag{11}$$

where g_e is the electron g-factor, λ is an effective SOC constant, $|\Psi\rangle$ is the orbital eigenstate under consideration with energy E_Ψ, $\{|\Psi'\rangle\}$ is the set of orbital eigenstates that is orthogonal to $|\Psi\rangle$ and has the energy spectrum $\{E_{\Psi'}\}$, and $\hat{L}_a$ is the a-th component of $\hat{\mathbf{L}}$, with the indices a and b running over all three-dimensional coordinates. Therefore, the interference effect can be chemically tuned by considering the symmetry of the photosensitizer.[86]

Other chemical knobs include the RP singlet−triplet gap, characterized by J, and the triplet RP decay, characterized by $V_{\text{SOC},+1}^{\text{RP-GS}}$. Their effects on χ are sketched in Figure 4b,c. In particular, as the RP singlet−triplet gap changes, the same maximum chiral resolution can be obtained at a different B_0 value. Also, perfect enantioseparation (i.e., 100% e.e.) can be achieved when $\pm V_{\text{SOC},+1}^{\text{RP-GS}}$ exactly equals $V_{\text{e,S}}^{\text{RP-GS}} \times [\langle {}^1\text{RP}|\hat{V}_s|{}^3\text{RP};+1\rangle/\Delta E_{T_{+1}-S}]$, which corresponds to either eqs 4 or 5 being zero. These observations will be crucial for future optimizations of the photosensitizer.

A Molecular Prototype. As a molecular prototype, we consider an axially chiral binaphthyl derivative NMI_2 adsorbed onto a $B(C_2F_5)_3$ photosensitizer [Figure 5a] and compute their properties using DFT and time-dependent DFT (TDDFT) (see Supporting Information S7, which cites refs 87−89). By choosing an organic system, we may expect the singlet−triplet RP coherence to live longer than its recombination to the GS.[14] An analogue, $B(C_2H_5)_3$, was previously proposed as a triplet photosensitizer[90] and we introduced fluorine substituents to bring its LUMO energy closer to the HOMO energy of NMI_2 [Figure 5b]. Indeed, the RP states form the lowest-lying singlet and triplet excited states [Figure 5c]. As for the photosensitizer's triplet LE, it appeared as the 33rd excited triplet state above other lower-lying triplet transitions [Figure 5c]. We expect these additional transitions to provide a ladder of triplet intermediate states for the rapid relaxation of the triplet LE following Kasha's rule.[77−79]

After forming the RP, the NMI_2 radical cation has a lower activation barrier to racemisation (0.72 eV) than the neutral molecule (1.10 eV). Their racemisation time scales are, respectively, in the order of 10 ms and 1 day at room temperature, estimated using transition state theory at a mode frequency of 1000 cm^{-1}.[91] Chemically, the RP racemises faster because an electron has been removed from the NMI_2 HOMO, which has a nodal plane around the dimer linkage [Figure 5d]. This creates a π-bond between the two aromatic subunits, thereby reducing the barrier to coplanarity in the transition state. For the same reason, the radical anion also has a lowered activation barrier of 0.64 eV—see Supporting Information S7.

All other parameters fall within our expectations: We find $|V_{\text{SOC},M_S}^{\text{RP-GS}}|$ to be around 0.5 cm^{-1} [Figure 5c], the ZFS parameters to be $D = -380$ MHz and $E = -96$ MHz, and the radical g-anisotropy to be around 10^{-4} (Supporting Information S7). If we approximate $J \approx -0.06$ cm^{-1}, $V_{\text{e,S}}^{\text{RP-GS}} \approx 100$ cm^{-1}, and $\Omega \approx 10^4$ cm^{-1}, values typical to organic systems,[14,76] then our analytical solution [eq 6] predicts maximum chiral resolutions χ of 19 and 0.054 at magnetic field strengths $|B_0|$ of 0.126 and 0.131 T respectively [Figure 5e]; both values correspond to an e.e. of 90%. As mentioned earlier, a perfect enantioselectivity of 100% e.e. can be engineered by using a different photosensitizer, which would modify Δg_{eff} and $V_{\text{SOC},M_S}^{\text{RP-GS}}$.

For simplicity, we have not considered ZFS or hyperfine coupling effects yet. None of these are expected to impact the chiral resolution significantly—see the next section and Supporting Information S3. We have also assumed a static molecular conformation and aligned the magnetic field perpendicularly to the $B(C_2F_5)_3$ plane. Nonetheless, we expect the chiral resolution to survive isotropic averaging given how the MFE is driven by g-anisotropy [eq 4]. Future works will also include the diffusive motion of the two subsystems, which is known to create CIDEP in RP chemistry.[1−7] Under such conditions, effects due to g-anisotropy might be weakened due to rotational diffusion,[8] an issue that can be tackled by trapping the photosensitizer on a surface or accelerating the RP decay through stronger SOCs.

Further Support Using the Lindblad Master Equation. To investigate the full photoexcitation-decay kinetics, we consider the time evolution of the system density operator $\hat{\rho}(t)$, modeled by a Lindblad master equation

$$\frac{d\hat{\rho}}{dt} = -\frac{i}{\hbar}[\hat{H},\hat{\rho}] + \sum_k \left(\hat{L}_k\hat{\rho}\hat{L}_k^{\dagger} - \frac{1}{2}\{\hat{L}_k^{\dagger}\hat{L}_k,\hat{\rho}\}\right) \tag{12}$$

The first term describes the coherent oscillations under a Hamiltonian $\hat{H}$ that comprises the state energies and the spin Hamiltonian, while the second term describes the bath-mediated processes through the jump operators $\hat{L}_k$. These bath-mediated processes include the triplet photoexcitation via

$$\hat{L}_{\text{pump}} = \sqrt{k_{\text{pump}}} \sum_{M_S=\pm1} |{}^3\text{LE};M_S\rangle\langle {}^1\text{GS}|$$

(see footnote[2]), the RP formation via

$$\hat{L}_{\text{LE}\to\text{RP},M_S} = V_{\text{e},M_S}^{\text{LE-RP}}/\sqrt{\hbar^2\Omega} \times |{}^3\text{RP};M_S\rangle\langle {}^3\text{LE};M_S|,$$

and the collective RP decay via

$$\hat{L}_{\text{RP}\to\text{GS}} = \frac{V_{\text{e,S}}^{\text{RP-GS}}}{\sqrt{\hbar^2\Omega}}|{}^1\text{GS}\rangle\langle {}^1\text{RP}| + \sum_{M_S=0,\pm1} \frac{V_{\text{SOC},M_S}^{\text{RP-GS}}}{\sqrt{\hbar^2\Omega}}|{}^1\text{GS}\rangle\langle {}^3\text{RP};M_S| \tag{13}$$

Also, every state is duplicated to describe the two enantiomers, which are linked through the RP states via the jump operator $\hat{L}_{\text{rac},m_{(X)}\to m_{(X')}} = \sqrt{k_{\text{rac}}}|m\rangle_{(X')\,(X)}\langle m|$, where X and X' denote opposite enantiomers, and m is a RP state

https://doi.org/10.1021/jacs.5c11502
J. Am. Chem. Soc. 2025, 147, 36579−36588

Table 1. Simulation Parameters in Units of cm^{-1}[a]

J	k_{pump}	$V_{e,M_S}^{LE\text{-}RP}$	$V_{SOC,\pm1}^{RP\text{-}GS}$	$V_{SOC,0}^{RP\text{-}GS}$	$V_{e,S}^{RP\text{-}GS}$	Ω	k_{rac}
−0.06	10^{-11}	10^{2}	$-0.37 \mp 0.34i$	$0.60i$	10^{2}	10^{4}	10^{-9}

[a]The **g** and **D** tensors are available in Supporting Information S7. The value of $V_{e,M_S}^{LE\text{-}RP}$ is the same for all three triplet M_S sublevels.

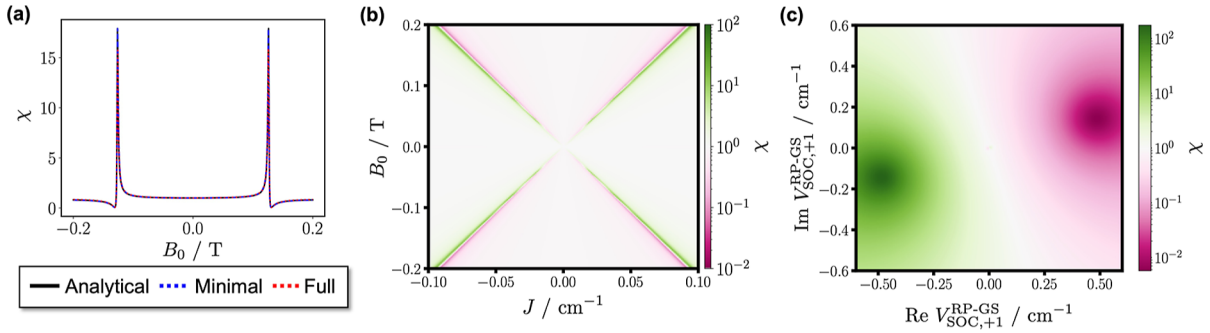

Figure 6. Numerical solution to the chiral resolution χ using the full Lindblad master equation, *neglecting* effects due to ZFS. The results are plotted across (a) the magnetic field strength, B_0, (b) the RP singlet−triplet gap, parametrized by J, and (c) the SOC matrix element $V_{SOC,+1}^{RP\text{-}GS}$ responsible for the triplet RP decay (B_0 = 0.126 T). In (c), the quantity χ approaches 187 (i.e., the e.e. reaches 99%) at the two large dots. Also presented in (a) are the results from the analytical [eq 6] and minimal three-level models.

[Figure 3]. As mentioned, metal-free RPs decay faster (at a time scale of microseconds) than their spins relax (milliseconds).[14] Hence, for simplicity, there are no spin relaxation pathways in our model.

We simulated the steady-state outcome numerically using $V_{e,M_S}^{LE\text{-}RP} \approx 100\ cm^{-1}$, $k_{pump} \approx (1\ s)^{-1}$ (i.e., a laser source), $k_{rac} \approx (10^{-2}\ s)^{-1}$, and other parameters as described before (Supporting Information S4, which cites ref 92). Table 1 summarizes the actual parameters used in our QuTiP script.[92] Strikingly, without ZFS, the chiral resolution χ matches the analytical predictions made earlier (Figures 6 versus 4), supporting our foregoing analysis. The enantioselectivity can also be perfected (i.e., the e.e. can also approach 100%) by tuning the photosensitizer structure, which would modify $V_{SOC,+1}^{RP\text{-}GS}$ [Figure 6c]. No major difference was observed when k_{pump} was set as $(1\ day)^{-1}$, corresponding to a mercury lamp source. We further develop a minimal three-level model comprising only the $|^1GS\rangle$, $|^1RP\rangle$, and $|^3RP;+1\rangle$ states (Supporting Information S5), which led to consistent results [Figure 6a]. Finally, even though the ZFS term introduces additional mixings among the triplet RP sublevels,[8] these sublevels decay independently from one another under the magnetic field. Therefore, the impact of ZFS on the chiral resolution is small, as confirmed by our numerical simulations [Figure 7].

Note that the collective form of $\hat{L}_{RP\to GS}$ [eq 13] is only fully justified if the four RP states have smaller energy separations (in frequency units) than their decay rates[82,83,90] (see footnote[3]). When any two RP states become nondegenerate (relative to the decay rate), the collective effect is partly penalised by the large energy gap,[80] although spurious interactions can still occur. This is particularly so in the $|B_0| \approx 0.01$ T regime of Figure 7, where we find small additional peaks that vanish when the decay channels involving nondegenerate RP states are more properly modeled by different jump operators (Supporting Information S4). To fully resolve this unphysical effect, we are currently working on a more systematic approach starting from a microscopic system-bath Hamiltonian.

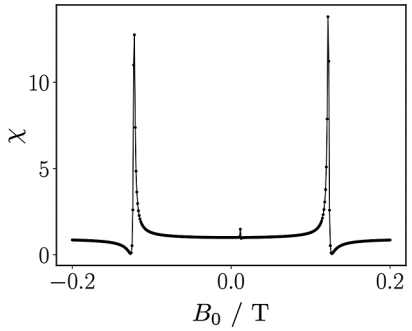

Figure 7. Chiral resolution χ at different magnetic field strengths B_0 as predicted by the full Lindblad master equation, *including* effects due to ZFS.

Estimated Time to Steady State. While this work focuses on the steady-state outcome, the time needed to achieve it is equally important. Under $k_{pump} \approx (1\ s)^{-1}$ for a teaching laboratory laser source,[84] enantioseparation occurs with a characteristic time scale of hundreds of milliseconds [Figure 8] and is experimentally achievable. Unfortunately, the time evolution of the density operator $\hat{\rho}(t)$ could not be solved for a lower k_{pump} of $(1\ day)^{-1}$, characteristic of a much lower intensity source such as a mercury lamp; this would be a more standard instrument in a synthetic chemistry laboratory. The underlying reason for this difficulty is the orders-of-magnitude differences in transition rates, resulting in an ill-conditioned rate constant matrix. As a preliminary solution, we consider a simplified kinetic scheme that assumes the stationary RP state in eq 3 to be formed prior to its recombination, which occurs within microseconds (Supporting Information S6). This yields a time scale toward steady state of around 10^4 days. Despite being experimentally unfeasible, this time scale is most likely overestimated because, in reality, the singlet and triplet RP states are evolving over time as they decay to the GS, and the former decays faster with a subnanosecond time scale. In Supporting Information S6, we explain how the time to steady

https://doi.org/10.1021/jacs.5c11502
J. Am. Chem. Soc. 2025, 147, 36579−36588

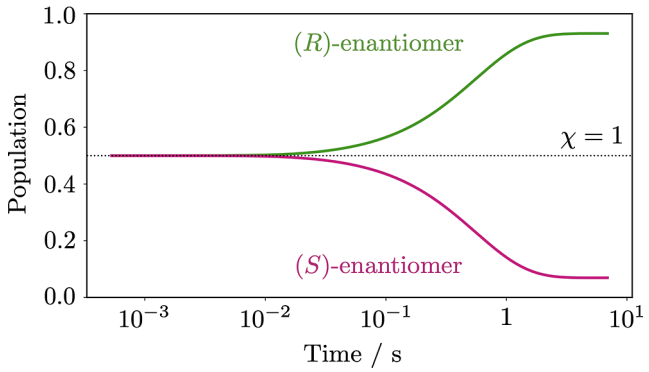

Figure 8. Time evolution of the enantiomer populations, defined as the trace of the density operator $\hat{\rho}(t)$ over the corresponding enantiomer subspace. These results are evaluated at $B_0 = 0.126$ T and $k_{pump} \approx (1\ s)^{-1}$ (i.e., a laser source).

state could potentially fall below 1 day once the full quantum master equations are considered, underscoring the limitation of our simple kinetic analysis. Work toward a more accurate quantum dynamics simulation is ongoing. Finally, we note that hyperfine coupling effects could prolong the time to steady state, although the new time scale remains experimentally realistic; see Supporting Information S6 for a full discussion.

Protocol Requirements. To summarize the requirements for our enantiopurification scheme, the criteria strictly necessary are as follows: (1) The RP states must be the lowest-lying excited states of the system, achieved by keeping the electron donor's HOMO at an energy close to the electron acceptor's LUMO. In experimental terms, this means that the donor's reduction potential should be close to the acceptor's reduction potential. (2) Chirality inversion in the RP states should occur with an appreciable rate relative to triplet excitation of the photosensitizer. In particular, relative to the present rates of around $(10\ ms)^{-1}$ and $1\ s^{-1}$, respectively, used in Figure 8 and Table 1, any decrease in the former will require a proportionate increase in the latter to sustain the same enantiopurification time scale. Next, the following features are not necessary but would improve the chiral resolution: (3) A photosensitizer embedded on a surface, which would minimize deleterious effects due to rotational averaging and RP diffusion while allowing for targeted excitation of the photosensitizer over the chiral molecule. (4) A nonmetallic photosensitizer, which would minimize loss of spin coherence, although this could be countered by a faster RP recombination rate achieved via stronger SOC from the metal.

CONCLUSION

Decades after establishing the link between mirror symmetry and TRS,[26,66−68] the magnetic field remains underutilized as a tool for chiral discrimination.[46−48,69] Our proposal offers a key step in this direction by leveraging on the well-established MFE in photogenerated RPs, which induces a collective decay to the ground state. Because the enantioselectivity relies on the SOC matrix elements, it can be chemically controlled through symmetry considerations of the photosensitizer.[86] In essence, our work exploits underexplored spin chemistry concepts to tackle the enantioselectivity problem critical in photoredox catalysis.[93−95] Given its generality and tunability, we expect this photoredox catalysis protocol to offer a novel concept for enantioseparation technology. Concurrently, we hope that this work will inspire other powerful ideas involving the use of spin dynamics to achieve unprecedented synthetic goals. In our future works, we will explore the consequences of isotropic averaging and enantioseparation kinetics, such as the role of RP diffusion in enhancing the spin polarization.[1−7] We will also devote much effort toward designing catalysts that can achieve the desired enantiopurification using the aforesaid low-intensity light sources, but within much shorter illumination times.

ASSOCIATED CONTENT

Supporting Information

The Supporting Information is available free of charge at https://pubs.acs.org/doi/10.1021/jacs.5c11502.

Theoretical methods, including the derivation of analytical results and ab initio procedures (PDF)

QuTiP script for numerical evaluation of Lindblad master equations (ZIP)

AUTHOR INFORMATION

Corresponding Authors

Yong Rui Poh − *Department of Chemistry and Biochemistry, University of California San Diego, La Jolla, California 92093, United States;* orcid.org/0009-0006-3648-3106; Email: ypoh@ucsd.edu

Joel Yuen-Zhou − *Department of Chemistry and Biochemistry, University of California San Diego, La Jolla, California 92093, United States;* orcid.org/0000-0002-8701-8793; Email: joelyuen@ucsd.edu

Authors

Arghadip Koner − *Department of Chemistry and Biochemistry, University of California San Diego, La Jolla, California 92093, United States*

Michael Reitz − *Department of Chemistry and Biochemistry, University of California San Diego, La Jolla, California 92093, United States*

Complete contact information is available at: https://pubs.acs.org/10.1021/jacs.5c11502

Author Contributions

‡Y.R.P. and A.K. contributed equally to this work.

Notes

The authors declare no competing financial interest.

ACKNOWLEDGMENTS

All authors were supported through the U.S. Department of Energy (DOE) under 2019030-SP DOE CalTech Sub S532207 (DESC0022089).

ADDITIONAL NOTES

[1]Examples include the Franck−Condon overlaps in the Marcus−Levich−Jortner models[77−79] and the bath component of the system-bath interaction in most quantum master equations.[80,81]

[2]We have omitted the triplet $M_S = 0$ transition because it is symmetry-forbidden in our photosensitizer.[90] However, the general conclusion does not change even after including the $M_S = 0$ triplet photoexcitation.

[3]The justification stems from the Bloch−Redfield equation, which can be rigorously derived from a microscopic system-bath Hamiltonian. To obtain the Lindblad jump operator in eq 13, the nonsecular Redfield terms responsible for the RP decay

must be kept with their transition energies approximated to be equal—see Supporting Information S4 and ref 80.

REFERENCES

(1) Adrian, F. J. Principles of the radical pair mechanism of chemically induced nuclear and electron spin polarization. *Rev. Chem. Intermed.* **1979**, *3*, 3−43.
(2) Murai, H. Spin-chemical approach to photochemistry: reaction control by spin quantum operation. *J. Photochem. Photobiol., C* **2003**, *3*, 183−201.
(3) Bargon, J. The inter-relationship between triplet energies and spin chemistry. *Photochem. Photobiol. Sci.* **2006**, *5*, 970−978.
(4) Kawai, A.; Shibuya, K. Electron spin dynamics in a pair interaction between radical and electronically-excited molecule as studied by a time-resolved ESR method. *J. Photochem. Photobiol., C* **2006**, *7*, 89−103.
(5) Yeganeh, S.; Wasielewski, M. R.; Ratner, M. A. Enhanced Intersystem Crossing in Three-Spin Systems: A Perturbation Theory Treatment. *J. Am. Chem. Soc.* **2009**, *131*, 2268−2273.
(6) Quintes, T.; Mayländer, M.; Richert, S. Properties and applications of photoexcited chromophore−radical systems. *Nat. Rev. Chem.* **2023**, *7*, 75−90.
(7) Zhang, C.; Ye, C.; Yao, J.; Wu, L.-Z. Spin-related excited-state phenomena in photochemistry. *Natl. Sci. Rev.* **2024**, *11*, nwae244.
(8) Atherton, N. M. *Principles of Electron Spin Resonance*; Physical Chemistry Series; Kemp, T. J., Ed.; Ellis Horwood, 1993.
(9) Ritz, T.; Thalau, P.; Phillips, J. B.; Wiltschko, R.; Wiltschko, W. Resonance effects indicate a radical-pair mechanism for avian magnetic compass. *Nature* **2004**, *429*, 177−180.
(10) Zhang, Y.; Berman, G. P.; Kais, S. The radical pair mechanism and the avian chemical compass: Quantum coherence and entanglement. *Int. J. Quantum Chem.* **2015**, *115*, 1327−1341.
(11) Hore, P. J.; Mouritsen, H. The Radical-Pair Mechanism of Magnetoreception. *Annu. Rev. Biophys.* **2016**, *45*, 299−344.
(12) Fay, T. P.; Lindoy, L. P.; Manolopoulos, D. E.; Hore, P. How quantum is radical pair magnetoreception? *Faraday Discuss.* **2020**, *221*, 77−91.
(13) Hasharoni, K.; Levanon, H.; Greenfield, S. R.; Gosztola, J.; Svec, W. A.; Wasielewski, M. R.; Wasielewski, M. R. Radical Pair and Triplet State Dynamics of a Photosynthetic Reaction-Center Model Embedded in Isotropic Media and Liquid Crystals. *J. Am. Chem. Soc.* **1996**, *118*, 10228−10235.
(14) Harvey, S. M.; Wasielewski, M. R. Photogenerated Spin-Correlated Radical Pairs: From Photosynthetic Energy Transduction to Quantum Information Science. *J. Am. Chem. Soc.* **2021**, *143*, 15508−15529.
(15) Lindoy, L. P.; Fay, T. P.; Manolopoulos, D. E. Quantum mechanical spin dynamics of a molecular magnetoreceptor. *J. Chem. Phys.* **2020**, *152*, 164107.
(16) Ray, K.; Ananthavel, S.; Waldeck, D.; Naaman, R. Asymmetric Scattering of Polarized Electrons by Organized Organic Films of Chiral Molecules. *Science* **1999**, *283*, 814−816.
(17) Evers, F.; Aharony, A.; Bar-Gill, N.; Entin-Wohlman, O.; Hedegård, P.; Hod, O.; Jelinek, P.; Kamieniarz, G.; Lemeshko, M.; Michaeli, K.; et al. Theory of Chirality Induced Spin Selectivity: Progress and Challenges. *Adv. Mater.* **2022**, *34*, 2106629.
(18) Aiello, C. D.; et al. A Chirality-Based Quantum Leap. *ACS Nano* **2022**, *16*, 4989−5035.
(19) Chiesa, A.; Privitera, A.; Macaluso, E.; Mannini, M.; Bittl, R.; Naaman, R.; Wasielewski, M. R.; Sessoli, R.; Carretta, S. Chirality-Induced Spin Selectivity: An Enabling Technology for Quantum Applications. *Adv. Mater.* **2023**, *35*, 2300472.
(20) Bloom, B. P.; Paltiel, Y.; Naaman, R.; Waldeck, D. H. Chiral Induced Spin Selectivity. *Chem. Rev.* **2024**, *124*, 1950−1991.
(21) Kondou, K.; Miwa, S.; Miyajima, D. Spontaneous spin selectivity in chiral molecules at the interface. *J. Magn. Magn. Mater.* **2023**, *585*, 171157.
(22) Göhler, B.; Hamelbeck, V.; Markus, T.; Kettner, M.; Hanne, G.; Vager, Z.; Naaman, R.; Zacharias, H. Spin Selectivity in Electron Transmission Through Self-Assembled Monolayers of Double-Stranded DNA. *Science* **2011**, *331*, 894−897.
(23) Abendroth, J. M.; Cheung, K. M.; Stemer, D. M.; El Hadri, M. S.; Zhao, C.; Fullerton, E. E.; Weiss, P. S. Spin-Dependent Ionization of Chiral Molecular Films. *J. Am. Chem. Soc.* **2019**, *141*, 3863−3874.
(24) Möllers, P. V.; Göhler, B.; Zacharias, H. Chirality Induced Spin Selectivity − the Photoelectron View. *Isr. J. Chem.* **2022**, *62*, No. e202200062.
(25) Wei, J.; Schafmeister, C.; Bird, G.; Paul, A.; Naaman, R.; Waldeck, D. Molecular Chirality and Charge Transfer through Self-Assembled Scaffold Monolayers. *J. Phys. Chem. B* **2006**, *110*, 1301−1308.
(26) Barron, L.; Vrbancich, J. Magneto-chiral birefringence and dichroism. *Mol. Phys.* **1984**, *51*, 715−730.
(27) Aragonès, A. C.; Medina, E.; Ferrer-Huerta, M.; Gimeno, N.; Teixidó, M.; Palma, J. L.; Tao, N.; Ugalde, J. M.; Giralt, E.; Díez-Pérez, I.; Mujica, V. Measuring the Spin-Polarization Power of a Single Chiral Molecule. *Small* **2017**, *13*, 1602519.
(28) Eckvahl, H. J.; Tcyrulnikov, N. A.; Chiesa, A.; Bradley, J. M.; Young, R. M.; Carretta, S.; Krzyaniak, M. D.; Wasielewski, M. R. Direct observation of chirality-induced spin selectivity in electron donor−acceptor molecules. *Science* **2023**, *382*, 197−201.
(29) Eckshtain-Levi, M.; Capua, E.; Refaely-Abramson, S.; Sarkar, S.; Gavrilov, Y.; Mathew, S. P.; Paltiel, Y.; Levy, Y.; Kronik, L.; Naaman, R. Cold denaturation induces inversion of dipole and spin transfer in chiral peptide monolayers. *Nat. Commun.* **2016**, *7*, 10744.
(30) Kumar, A.; Capua, E.; Kesharwani, M. K.; Martin, J. M.; Sitbon, E.; Waldeck, D. H.; Naaman, R. Chirality-induced spin polarization places symmetry constraints on biomolecular interactions. *Proc. Natl. Acad. Sci. U.S.A.* **2017**, *114*, 2474−2478.
(31) Ben Dor, O.; Yochelis, S.; Radko, A.; Vankayala, K.; Capua, E.; Capua, A.; Yang, S.-H.; Baczewski, L. T.; Parkin, S. S. P.; Naaman, R.; Paltiel, Y. Magnetization switching in ferromagnets by adsorbed chiral molecules without current or external magnetic field. *Nat. Commun.* **2017**, *8*, 14567.
(32) Wu, Y.; Miao, G.; Subotnik, J. E. Chemical Reaction Rates for Systems with Spin−Orbit Coupling and an Odd Number of Electrons: Does Berry's Phase Lead to Meaningful Spin-Dependent Nuclear Dynamics for a Two State Crossing? *J. Phys. Chem. A* **2020**, *124*, 7355−7372.
(33) Zhang, L.; Hao, Y.; Qin, W.; Xie, S.; Qu, F. Chiral-induced spin selectivity: A polaron transport model. *Phys. Rev. B* **2020**, *102*, 214303.
(34) Das, T. K.; Tassinari, F.; Naaman, R.; Fransson, J. Temperature-Dependent Chiral-Induced Spin Selectivity Effect: Experiments and Theory. *J. Phys. Chem. C* **2022**, *126*, 3257−3264.
(35) Kato, A.; Yamamoto, H. M.; Kishine, J.-i. Chirality-induced spin filtering in pseudo Jahn-Teller molecules. *Phys. Rev. B* **2022**, *105*, 195117.
(36) Barroso, M.; Balduque, J.; Domínguez-Adame, F.; Díaz, E. Spin-dependent polaron transport in helical molecules. *Appl. Phys. Lett.* **2022**, *121*, 143505.
(37) Klein, D.; Michaeli, K. Giant chirality-induced spin selectivity of polarons. *Phys. Rev. B* **2023**, *107*, 045404.
(38) Vittmann, C.; Lim, J.; Tamascelli, D.; Huelga, S. F.; Plenio, M. B. Spin-Dependent Momentum Conservation of Electron−Phonon Scattering in Chirality-Induced Spin Selectivity. *J. Phys. Chem. Lett.* **2023**, *14*, 340−346.
(39) Fathizadeh, S. Phonon-assisted nearly pure spin current in DNA molecular chains: a multifractal analysis. *Sci. Rep.* **2023**, *13*, 21281.
(40) Chen, S.; Wu, R.; Fu, H.-H. Persistent Chirality-Induced Spin-Selectivity Effect in Circular Helix Molecules. *Nano Lett.* **2024**, *24*, 6210−6217.
(41) Chiesa, A.; Garlatti, E.; Mezzadri, M.; Celada, L.; Sessoli, R.; Wasielewski, M. R.; Bittl, R.; Santini, P.; Carretta, S. Many-Body Models for Chirality-Induced Spin Selectivity in Electron Transfer. *Nano Lett.* **2024**, *24*, 12133−12139.

https://doi.org/10.1021/jacs.5c11502
J. Am. Chem. Soc. 2025, 147, 36579−36588

(42) Varela, S.; Gutierrez, R.; Cuniberti, G.; Medina, E.; Mujica, V. Chiral spin selectivity and chiroptical activity in helical molecules. *J. Chem. Phys.* **2024**, *161*, 114111.
(43) Fransson, J.; Kapon, Y.; Brann, L.; Yochelis, S.; Sasselov, D. D.; Paltiel, Y.; Ozturk, S. F. Chiral Phonons Enhance Ferromagnetism. *J. Phys. Chem. Lett.* **2025**, *16*, 2001−2007.
(44) Shiranzaei, M.; Kalhöfer, S.; Fransson, J. Emergent Magnetism as a Cooperative Effect of Interactions and Reservoir. *J. Phys. Chem. Lett.* **2023**, *14*, 5119−5126.
(45) Zöllner, M. S.; Saghatchi, A.; Mujica, V.; Herrmann, C. Influence of Electronic Structure Modeling and Junction Structure on First-Principles Chiral Induced Spin Selectivity. *J. Chem. Theory Comput.* **2020**, *16*, 7357−7371.
(46) Bloom, B.; Lu, Y.; Metzger, T.; Yochelis, S.; Paltiel, Y.; Fontanesi, C.; Mishra, S.; Tassinari, F.; Naaman, R.; Waldeck, D. Asymmetric reactions induced by electron spin polarization. *Phys. Chem. Chem. Phys.* **2020**, *22*, 21570−21582.
(47) Naaman, R.; Paltiel, Y.; Waldeck, D. H. Chiral Induced Spin Selectivity Gives a New Twist on Spin-Control in Chemistry. *Acc. Chem. Res.* **2020**, *53*, 2659−2667.
(48) Ma, S.; Lee, H.; Moon, J. Chirality-Induced Spin Selectivity Enables New Breakthrough in Electrochemical and Photoelectrochemical Reactions. *Adv. Mater.* **2024**, *36*, 2405685.
(49) Banerjee-Ghosh, K.; Ben Dor, O.; Tassinari, F.; Capua, E.; Yochelis, S.; Capua, A.; Yang, S.-H.; Parkin, S. S. P.; Sarkar, S.; Kronik, L.; Baczewski, L. T.; Naaman, R.; Paltiel, Y. Separation of enantiomers by their enantiospecific interaction with achiral magnetic substrates. *Science* **2018**, *360*, 1331−1334.
(50) Tassinari, F.; Steidel, J.; Paltiel, S.; Fontanesi, C.; Lahav, M.; Paltiel, Y.; Naaman, R. Enantioseparation by crystallization using magnetic substrates. *Chem. Sci.* **2019**, *10*, 5246−5250.
(51) Bhowmick, D.; Sang, Y.; Santra, K.; Halbauer, M.; Capua, E.; Paltiel, Y.; Naaman, R.; Tassinari, F. Simultaneous High-Purity Enantiomeric Resolution of Conglomerates Using Magnetic Substrates. *Cryst. Growth Des.* **2021**, *21*, 2925−2931.
(52) Lu, Y.; Bloom, B.; Qian, S.; Waldeck, D. Enantiospecificity of Cysteine Adsorption on a Ferromagnetic Surface: Is It Kinetically or Thermodynamically Controlled? *J. Phys. Chem. Lett.* **2021**, *12*, 7854−7858.
(53) Ozturk, S. F.; Liu, Z.; Sutherland, J. D.; Sasselov, D. D. Origin of biological homochirality by crystallization of an RNA precursor on a magnetic surface. *Sci. Adv.* **2023**, *9*, No. eadg8274.
(54) Lu, Y.; Qiu, T.; Bloom, B. P.; Subotnik, J. E.; Waldeck, D. H. Spin-Based Chiral Separations and the Importance of Molecule−Solvent Interactions. *J. Phys. Chem. C* **2023**, *127*, 14155−14162.
(55) Ozturk, S. F.; Sasselov, D. D. On the origins of life's homochirality: Inducing enantiomeric excess with spin-polarized electrons. *Proc. Natl. Acad. Sci. U.S.A.* **2022**, *119*, No. e2204765119.
(56) Kapon, Y.; Brann, L.; Yochelis, S.; Fransson, J.; Sasselov, D. D.; Paltiel, Y.; Ozturk, S. F. Non-classical Temperature Dependence of Chirality-Induced Magnetization and Its Implications for RNA's Homochirality. *arXiv* **2024**, arXiv:2412.05720.
(57) Dianat, A.; Gutierrez, R.; Alpern, H.; Mujica, V.; Ziv, A.; Yochelis, S.; Millo, O.; Paltiel, Y.; Cuniberti, G. Role of Exchange Interactions in the Magnetic Response and Intermolecular Recognition of Chiral Molecules. *Nano Lett.* **2020**, *20*, 7077−7086.
(58) Wang, C.; Guo, A.-M.; Sun, Q.-F.; Yan, Y. Efficient Spin-Dependent Charge Transmission and Improved Enantioselective Discrimination Capability in Self-Assembled Chiral Coordinated Monolayers. *J. Phys. Chem. Lett.* **2021**, *12*, 10262−10269.
(59) Fransson, J. Charge and Spin Dynamics and Enantioselectivity in Chiral Molecules. *J. Phys. Chem. Lett.* **2022**, *13*, 808−814.
(60) Buchardt, O. Photochemistry with circularly polarized light. *Angew. Chem., Int. Ed.* **1974**, *13*, 179−185.
(61) Huck, N. P.; Jager, W. F.; De Lange, B.; Feringa, B. L. Dynamic Control and Amplification of Molecular Chirality by Circular Polarized Light. *Science* **1996**, *273*, 1686−1688.
(62) Kawasaki, T.; Sato, M.; Ishiguro, S.; Saito, T.; Morishita, Y.; Sato, I.; Nishino, H.; Inoue, Y.; Soai, K. Enantioselective Synthesis of Near Enantiopure Compound by Asymmetric Autocatalysis Triggered by Asymmetric Photolysis with Circularly Polarized Light. *J. Am. Chem. Soc.* **2005**, *127*, 3274−3275.
(63) Hashim, P.; Tamaoki, N. Enantioselective Photochromism under Circularly Polarized Light. *ChemPhotoChem* **2019**, *3*, 347−355.
(64) Rijeesh, K.; Hashim, P.; Noro, S.-i.; Tamaoki, N. Dynamic induction of enantiomeric excess from a prochiral azobenzene dimer under circularly polarized light. *Chem. Sci.* **2015**, *6*, 973−980.
(65) Dalum, S.; Hedegård, P. Theory of Chiral Induced Spin Selectivity. *Nano Lett.* **2019**, *19*, 5253−5259.
(66) Baranova, N.; Bogdanov, Y. V.; Zel'Dovich, B. Y. Electrical analog of the Faraday effect and other new optical effects in liquids. *Opt. Commun.* **1977**, *22*, 243−247.
(67) Wagnière, G.; Meier, A. The influence of a static magnetic field on the absorption coefficient of a chiral molecule. *Chem. Phys. Lett.* **1982**, *93*, 78−81.
(68) Rikken, G.; Raupach, E. Observation of magneto-chiral dichroism. *Nature* **1997**, *390*, 493−494.
(69) Rikken, G.; Raupach, E. Enantioselective magnetochiral photochemistry. *Nature* **2000**, *405*, 932−935.
(70) Xu, Y.; Yang, G.; Xia, H.; Zou, G.; Zhang, Q.; Gao, J. Enantioselective synthesis of helical polydiacetylene by application of linearly polarized light and magnetic field. *Nat. Commun.* **2014**, *5*, 5050.
(71) Atzori, M.; Rikken, G. L.; Train, C. Magneto-Chiral Dichroism: A Playground for Molecular Chemists. *Chem.—Eur. J.* **2020**, *26*, 9784−9791.
(72) Atzori, M.; Santanni, F.; Breslavetz, I.; Paillot, K.; Caneschi, A.; Rikken, G. L.; Sessoli, R.; Train, C. Magnetic Anisotropy Drives Magnetochiral Dichroism in a Chiral Molecular Helix Probed with Visible Light. *J. Am. Chem. Soc.* **2020**, *142*, 13908−13916.
(73) Ishii, K.; Hattori, S.; Kitagawa, Y. Recent advances in studies on the magneto-chiral dichroism of organic compounds. *Photochem. Photobiol. Sci.* **2020**, *19*, 9−19.
(74) Atzori, M.; Ludowieg, H.; Valentín-Pérez, Á.; Cortijo, M.; Breslavetz, I.; Paillot, K.; Rosa, P.; Train, C.; Autschbach, J.; Hillard, E.; Rikken, G. Validation of microscopic magnetochiral dichroism theory. *Sci. Adv.* **2021**, *7*, No. eabg2859.
(75) Fay, T. P. Chirality-Induced Spin Coherence in Electron Transfer Reactions. *J. Phys. Chem. Lett.* **2021**, *12*, 1407−1412.
(76) Fay, T. P.; Limmer, D. T. Origin of Chirality Induced Spin Selectivity in Photoinduced Electron Transfer. *Nano Lett.* **2021**, *21*, 6696−6702.
(77) Englman, R.; Jortner, J. The energy gap law for radiationless transitions in large molecules. *Mol. Phys.* **1970**, *18*, 145−164.
(78) Poh, Y. R.; Pannir-Sivajothi, S.; Yuen-Zhou, J. Understanding the Energy Gap Law under Vibrational Strong Coupling. *J. Phys. Chem. C* **2023**, *127*, 5491−5501.
(79) Ramos, P.; Friedman, H.; Li, B. Y.; Garcia, C.; Sletten, E.; Caram, J. R.; Jang, S. J. Nonadiabatic Derivative Couplings through Multiple Franck−Condon Modes Dictate the Energy Gap Law for Near and Short-Wave Infrared Dye Molecules. *J. Phys. Chem. Lett.* **2024**, *15*, 1802−1810.
(80) Breuer, H.-P.; Petruccione, F. *The Theory of Open Quantum Systems*; Oxford University Press, 2002; Chapter 3, pp 109−218.
(81) Nitzan, A. *Chemical Dynamics in Condensed Phases: Relaxation, Transfer and Reactions in Condensed Molecular Systems*; Oxford University Press, 2006; Chapter 10, pp 347−398.
(82) Baryshnikov, G.; Minaev, B.; Ågren, H. Theory and Calculation of the Phosphorescence Phenomenon. *Chem. Rev.* **2017**, *117*, 6500−6537.
(83) Yuan, J.; Chen, R.; Tang, X.; Tao, Y.; Xu, S.; Jin, L.; Chen, C.; Zhou, X.; Zheng, C.; Huang, W. Direct population of triplet excited states through singlet−triplet transition for visible-light excitable organic afterglow. *Chem. Sci.* **2019**, *10*, 5031−5038.
(84) Zhang, H.; Belvin, C.; Li, W.; Wang, J.; Wainwright, J.; Berg, R.; Bridger, J. Little bits of diamond: Optically detected magnetic resonance of nitrogen-vacancy centers. *Am. J. Phys.* **2018**, *86*, 225−236.

(85) Tscherbul, T. V.; Brumer, P. Long-Lived Quasistationary Coherences in a V-type System Driven by Incoherent Light. *Phys. Rev. Lett.* **2014**, *113*, 113601.
(86) Poh, Y. R.; Yuen-Zhou, J. Enhancing the Optically Detected Magnetic Resonance Signal of Organic Molecular Qubits. *ACS Cent. Sci.* **2025**, *11*, 116−126.
(87) Grimme, S.; Antony, J.; Ehrlich, S.; Krieg, H. A consistent and accurate ab initio parametrization of density functional dispersion correction (DFT-D) for the 94 elements H-Pu. *J. Chem. Phys.* **2010**, *132*, 154104.
(88) Grimme, S.; Ehrlich, S.; Goerigk, L. Effect of the damping function in dispersion corrected density functional theory. *J. Comput. Chem.* **2011**, *32*, 1456−1465.
(89) Neese, F. Software update: The ORCA program system-Version 5.0. *WIREs Comput. Mol. Sci.* **2022**, *12*, No. e1606.
(90) Szumska, A. A.; Sirringhaus, H.; Nelson, J. Symmetry based molecular design for triplet excitation and optical spin injection. *Phys. Chem. Chem. Phys.* **2019**, *21*, 19521−19528.
(91) Nitzan, A. *Chemical Dynamics in Condensed Phases: Relaxation, Transfer and Reactions in Condensed Molecular Systems*; Oxford University Press, 2006; Chapter 14, pp 483−535.
(92) Johansson, J. R.; Nation, P. D.; Nori, F. QuTiP: An open-source Python framework for the dynamics of open quantum systems. *Comput. Phys. Commun.* **2012**, *183*, 1760−1772.
(93) Romero, N. A.; Nicewicz, D. A. Organic Photoredox Catalysis. *Chem. Rev.* **2016**, *116*, 10075−10166.
(94) Genzink, M. J.; Kidd, J. B.; Swords, W. B.; Yoon, T. P. Chiral Photocatalyst Structures in Asymmetric Photochemical Synthesis. *Chem. Rev.* **2022**, *122*, 1654−1716.
(95) Chan, A. Y.; et al. Metallaphotoredox: The Merger of Photoredox and Transition Metal Catalysis. *Chem. Rev.* **2022**, *122*, 1485−1542.

https://doi.org/10.1021/jacs.5c11502
J. Am. Chem. Soc. 2025, 147, 36579−36588